Acta Materialia 188 (2020) 376–385

Contents lists available at ScienceDirect

Acta Materialia

journal homepage: www.elsevier.com/locate/actamat

Full length article

EBSD orientation analysis based on experimental Kikuchi reference patterns

Aimo Winkelmann[a,c,d,*], Grzegorz Cios[a], Tomasz Tokarski[a], Gert Nolze[f,e], Ralf Hielscher[b], Tomasz Kozieł[g]

[a] Academic Centre for Materials and Nanotechnology, AGH University of Science and Technology, al. A. Mickiewicza 30, 30-059 Krakow, Poland
[b] Department of Mathematics, Technical University Chemnitz, Reichenhainer Straße 39, 09126 Chemnitz, Germany
[c] Laser Zentrum Hannover e.V., Hollerithallee 8, 30419 Hannover , Germany
[d] Department of Physics, SUPA, University of Strathclyde, Glasgow G4 0NG, United Kingdom
[e] TU Bergakademie Freiberg, Institute for Mineralogy, Brennhausgasse 14, 09596 Freiberg, Germany
[f] Federal Institute for Materials, Research and Testing (BAM), Unter den Eichen 87, 12205 Berlin, Germany
[g] Faculty of Metals and Industrial Computer Science, AGH University of Science and Technology, al. A. Mickiewicza 30, 30-059 Krakow, Poland

ARTICLE INFO

Article History:
Received 13 November 2019
Revised 17 January 2020
Accepted 26 January 2020
Available online 11 February 2020

Keywords:
EBSD
Quasicrystal
Crystal orientation
Pattern matching

ABSTRACT

Orientation determination does not necessarily require complete knowledge of the local atomic arrangement in a crystalline phase. We present a method for microstructural phase discrimination and orientation analysis of phases for which there is only limited crystallographic information available. In this method, experimental Kikuchi diffraction patterns are utilized to generate a self-consistent master reference for use in the technique of Electron Backscatter Diffraction (EBSD). The experimentally derived master data serves as an application-specific reference in EBSD pattern matching approaches. As application examples, we map the locally varying orientations in samples of icosahedral quasicrystals observed in a Ti40Zr40Ni20 alloy, and we analyse AlNiCo decagonal quasicrystals.

1. Introduction

The characterization of the microstructure of materials provides important information for the understanding of their properties. In this context, electron backscatter diffraction (EBSD) is a useful tool for sub-micron-scale crystallographic analysis of materials in the scanning electron microscope (SEM) [1]. EBSD delivers spatially resolved crystallographic information via measurement of backscattered Kikuchi diffraction (BKD) patterns that are formed by incoherent point sources of backscattered electrons within a single crystalline volume [2]. Compared to other diffraction techniques, Kikuchi patterns have the distinct advantage that they provide a rather extended, wide-angle view on potential point group symmetries of the phase that is probed locally by the incident electron beam.

If the crystal structure of the phases in the material is known, the properties of the corresponding Kikuchi patterns can be approximated using different theoretical models [3], and the local orientation can be determined by comparison of experimental Kikuchi pattern features to crystallographic predictions. In the analysis of microstructures in the SEM, however, it can often be desirable to obtain orientational information even from phases for which we have only a limited knowledge about their actual crystal structure.

In favorable cases, the EBSD system software can still be used for orientation determination even of unknown phases, due to the fact that the experimental Kikuchi pattern is reduced basically to a set of linear features extracted by the Hough transform as one of the first steps of the EBSD data processing pipeline [4]. While, on the one hand, the geometrical image analysis of Kikuchi patterns by the Hough transform is limiting the sensitivity of EBSD systems in terms of correct phase *discrimination*, it can also be seen, on the other hand, to provide some flexibility in terms of orientation analysis. A realistic example would be the analysis of an unknown metal alloy using a commercial EBSD system, which could be accomplished by randomly including various known *fcc* and *bcc* phases in the phase list of the indexing software if the unknown alloy is expected to be approximately cubic. Because the interplanar angles are the same for all cubic phases, the EBSD system will often still index the unknown phase and provide orientation information even if the phase is assigned incorrectly and remains unknown. While the inclusion of such proxy phases provides a way to alleviate some problems due to the indexing limits of an EBSD system, this comes at the price of neglecting a

* Corresponding author at: Academic Centre for Materials and Nanotechnology, AGH University of Science and Technology, al. A. Mickiewicza 30, 30-059 Krakow, Poland.
E-mail address: winkelmann@agh.edu.pl (A. Winkelmann).

https://doi.org/10.1016/j.actamat.2020.01.053

major fraction of the detailed intensity information in EBSD Kikuchi patterns in terms of the orientation precision and phase discrimination which these patterns could potentially provide.

For high-precision orientation analyses by EBSD, pattern matching approaches apply a quantitative comparison of experimentally collected diffraction patterns with data simulated according to a theoretical crystal structure and additional physical parameters. While advanced Kikuchi pattern simulations [5–7] are extremely useful for a comparison to known structures, the application of such simulated patterns is limited by the knowledge of the crystal structure itself, but also by the ancillary parameters which determine the quantitative development of Kikuchi diffraction patterns from a specific material. Even for known crystal structures, specific experimental effects can be very characteristic in a Kikuchi pattern but expensive to simulate at the same time. This includes, for example, features due to higher order Laue zone (HOLZ) rings [8], which can be very distinctive for a specific phase and electron energy.

In order to circumvent some of the aforementioned problems related to quantitative Kikuchi pattern simulations for arbitrary phases, we present an approach which generates a global reference master pattern from a number of experimentally measured Kikuchi diffraction patterns and subsequently uses this Kikuchi master pattern as the reference for a precise orientation determination. This type of approach can be compared with the use of experimental reference X-ray spectra in standards-based microanalysis in the SEM [9]. A precise knowledge of the underlying atomic crystal structure is not needed for EBSD orientation determination based on experimental reference data, as is illustrated by earlier, non-automated, attempts on phase and orientation determination using atlases of Kikuchi pattern "fingerprints" in the absence of any sufficiently realistic simulations [10,11].

The example application which we discuss in this paper concerns the local orientation determination in grains of quasicrystalline materials, which can provide additional information for the understanding of the formation of such materials with respect to different crystallization conditions or casting techniques [12–15]. It is well known that quasicrystals and closely related structures form Kikuchi patterns, which convey structural information even in the absence of long-range three-dimensional crystalline order [16–21]. As we will show below, the EBSD approach discussed in this paper can reveal precise microstructural details on length scales down to the subgrain level of quasicrystalline materials. Apart from our specific demonstration example, EBSD based on experimental reference data can be applied to a wide range of materials. Since the global reference pattern is derived directly from an experimental signal, it provides an alternative method for phase discrimination and orientation analysis which is not based on the use of pattern simulations.

2. Experimental

2.1. Materials and casting

A mixture of high-purity elements with a composition of Ti40Zr40Ni20 has been arc melted in a high vacuum evacuated argon atmosphere using an Arc Melter AM (Edmund Bühler GmbH). The sample was produced by suction casting into a copper mould of ø = 6 mm and a length of 55 mm [22]. Composition and casting technique are based on studies published in [23]. The EBSD analyses were performed in cross-sections, i.e. in planes perpendicular to the cylindrical axis (∥ Z). The sample reflects a typical cast structure of quasicrystalline grains with icosahedral symmetry.

The decagonal AlCoNi quasicrystals have been grown from Al-rich melts [24] using the Czochralski method. The investigated sample area contained a secondary phase, Al_3Ni, beside the main quasicrystalline phase.

2.2. EBSD pattern acquisition

For the orientation mapping of the icosahedral quasicrystals, patterns with a resolution of 120 × 120 pixels have been acquired using a Hikari detector (EDAX). An averaging of three patterns resulted in an effective dwell time of 30 ms/point. The detector was mounted on a Versa 3D (FEI) field-emission scanning electron microscope (FE-SEM) which was operated at 20 kV acceleration voltage and 32 nA beam current.

The decagonal quasicrystals (AlCoNi) have been investigated in a LEO 1530VP FE-SEM (Zeiss) operated at 20 kV with a beam current of ≈ 11 nA. The EBSD patterns of the e⁻Flash^{HR} detector (Bruker Nano) were binned down to an image size of 160 × 115 pixels, the dwell time per pattern was 20ms. The raw EBSD patterns were stored for subsequent data analyses.

2.3. Experimental Kikuchi diffraction reference

Kikuchi pattern features, such as Kikuchi bands and their intersections, directly correlate with the gnomonic projection of crystallographic features such as lattice planes (hkl) and zone axes [uvw] on the planar phosphor screen. The lattice plane traces are related to the centers of Kikuchi bands, and lattice directions correspond to their intersections [26]. Changes in these geometrically defined features of Kikuchi patterns can thus be linked to changes in the projection geometry, to lattice rotations, and to variations in the lattice parameter ratios [27].

If we can identify crystallographic reference directions (symmetry axes) in an experimental Kikuchi pattern, we can thus also derive a cartesian crystal reference system [28] from these observed directions. In this way, we can determine local crystallographic changes by comparison to purely experimental reference patterns. This especially includes local rotations in the observed sample, i.e. orientations and misorientations. Because the experimental Kikuchi pattern reference is energy-, phase- and material-specific, phase discrimination in general will also profit from this approach, with the experiment providing an empirical fingerprint of the phase which can be matched against measured patterns.

The generation of the experimental Kikuchi master reference is illustrated in Fig. 1 for an icosahedral quasicrystal observed in a Ti40Zr40Ni20 (at%) alloy. In panel (b), we show an experimental Kikuchi pattern with two-fold, three-fold, and five-fold rotation axes marked. With respect to the icosahedral point group [25], we reprojected the experimental data from (b) to the complete hemisphere as shown in the stereographic projection in (a). This setting has two-fold axes of the icosahedron along the cartesian X,Y,Z reference axes. In Fig. 1 a, the upper hemisphere is limited by the circle with unit radius, points outside this radius belong to the lower hemisphere.

For the points **p** in the stereographic projection of the master reference pattern, we use a projective transformation to determine the intensity at the corresponding point **q** in the gnomonic projection of the experimental pattern. The point **p** in the stereographic projection corresponds to a vector $(x^p, y^p, z^p)^T$, and a projective transformation **H** results in the homogeneous coordinates $\lambda^q(x_E^q, y_E^q, 1)^T$, with x_E^q and y_E^q as the experimental 2D pattern coordinates of the point **q**:

$$\lambda^q \begin{bmatrix} x_E^q \\ y_E^q \\ 1 \end{bmatrix} = \mathbf{H} \begin{bmatrix} x^p \\ y^p \\ z^p \end{bmatrix} \quad (1)$$

The experimental pattern coordinates (x_E^q, y_E^q) are obtained by normalization of the transformation result to the third coordinate λ^q. The projective (3 × 3) transformation **H** is determined by the correspondences of at least 4 suitable point pairs [29]. In our case, we use the 4 observed **q**-points **a, b, c, d** of the symmetry axes as measured in the experimental data in Fig. 1(b) and the corresponding **p**-reference directions **A, B, C,**

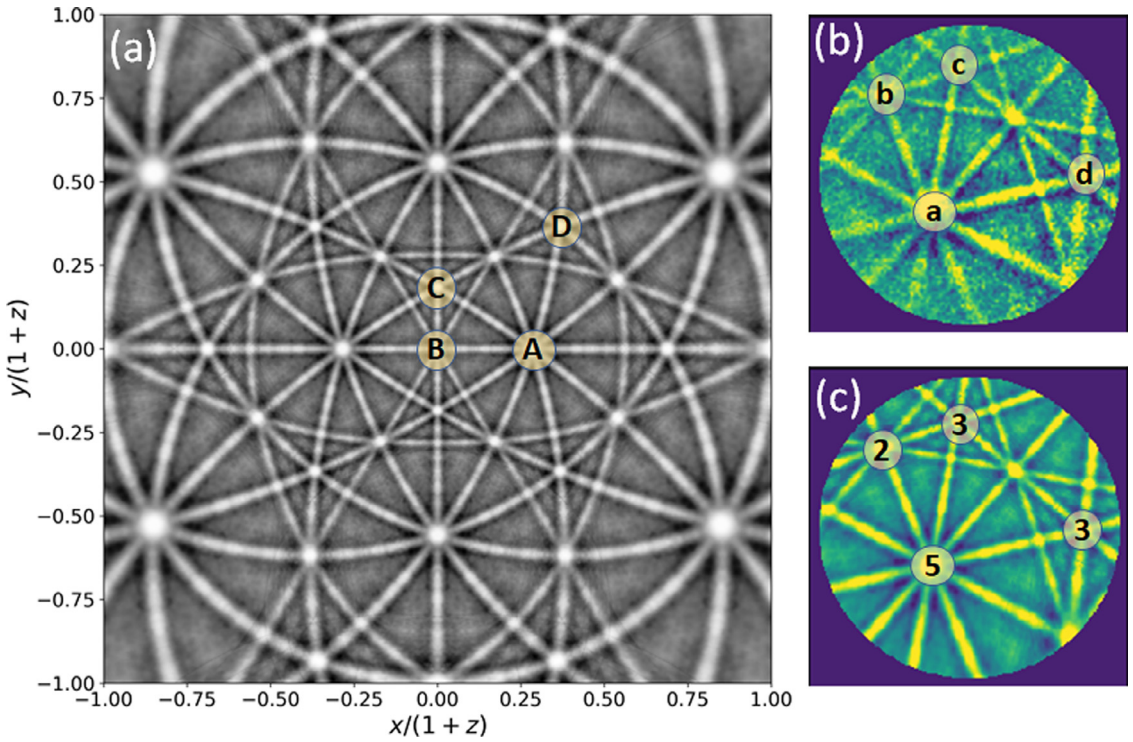

Fig. 1. (a) Stereographically projected Kikuchi diffraction master reference for quasicrystals formed in Ti40Zr40Ni20. The master reference (a) is generated from the experimental pattern in (b) by a projective transformation determined by 4 corresponding point pairs and symmetrization according to the icosahedral symmetry [25], (c) represents the best-fit reprojected pattern from the master reference shown in (a), with symmetry axes indicated. The normalized cross correlation coefficient is $r = 0.76$ between the patterns shown in (b) and (c).

D in Fig. 1(a) as given by the setting of the icosahedral group in [25]. Because **H** has 8 degrees of freedom, scaling of **H** by a real factor does not change the projective transformation [29]. By use of the icosahedral symmetry, the full stereographic projection can be assembled from the experimental data. We note that the experimental EBSD projection center [30,31] is implicitly contained in the projective transformation defined by the 4-point correspondence and can be obtained by a corresponding decomposition of **H** [27].

For the present application, the determination of the position of the symmetry axes in the experimental patterns has been carried out manually by visually judging a best fit position for the zone axes as intersections of Kikuchi bands. As will be shown below in Section 3.2, the manual procedure already leads to a very good orientation precision in the order of 0.1° in the final result. For future applications, the automated generation of the experimental master reference can be imagined, which could be alternatively based on the positions of Kikuchi bands in order to define the position of zone axes more precisely [26]. Such automated procedures will benefit from image registration algorithms [32] and from the determination of best-fit projective transformations from more than the minimum of 4 point correspondences required. In addition, the calibration of the standard can be improved by including models for the lens distortions in the optical system of the EBSD camera [33].

After the reprojection and symmetrization discussed in the previous paragraphs, the experimental data for the Kikuchi sphere [34–37] can serve as the global master data for the subsequent pattern matching [38,39], bypassing theoretical simulations of the observed quasicrystal Kikuchi patterns. The use of higher-dimensional lattices for a full crystallographic analysis of quasicrystals [40] is not required in our approach, which is limited to orientation determination. As a side effect of the reprojection, the symmetrization of the experimental data also results in a reduction of noise, as can be seen by the reprojected Kikuchi pattern in Fig. 1(c). A comparison to the original pattern in Fig. 1(b) indicates that the low noise reprojection provides an optimized template for pattern matching. Quantitatively, the similarity between the original and the reprojected pattern is characterized by a normalized cross correlation coefficient of $r = 0.76$, which indicates a very good fit according to previous studies for various other materials [39,41–43].

In comparison to the icosahedral Kikuchi master reference shown in Fig. 1, the number of symmetry elements can be severely reduced for arbitrary other crystalline phases. In these cases, it will often be necessary to assemble the experimental Kikuchi master reference from a sufficient number of calibrated experimental patterns. This is straightforward as long as the overlap between the measured patterns allows to identify the corresponding features on the Kikuchi sphere [37], which can be assembled from a number of Kikuchi patterns measured in a calibrated geometry. Once the experimental Kikuchi master reference has been obtained, however, EBSD pattern matching approaches operate in a similar way with structures of any symmetry, enabling phase discrimination and orientation analysis. Seen from a more general perspective, an orientation analysis approach based on experimental master references can be expected to work when each experimental observation can be approximately derived from a projection of a rotated spherical master reference. This includes, for example, Kossel patterns in X-ray diffraction [44,45].

2.4. Orientation determination and visualization

The rotations of the quasicrystal are defined relative to a reference orientation with the cartesian axes of the quasicrystal aligned with the corresponding sample system directions [28]. For the orientation mapping, we determined an initial orientation description for each measurement point by a brute-force template matching approach similar to the one described in [38]. We used a predefined set of diffraction pattern templates which covered the orientations of the point group 235 with an orientation resolution of 2.5°. The local projection centers have been determined for each map position

according to a projective model of the SEM beam scan on the tilted sample plane [28]. For the final, high-precision orientation refinement, we applied nonlinear optimization using real-time reprojection [39] of diffraction data and with starting values determined by the initial brute-force pattern matching step. In the pattern matching, the best fit is selected by the largest value of the normalized cross-correlation coefficient r [46] between the background-processed experimental pattern and the template derived from the Kikuchi master reference [43]. The presentation of the orientation results is based on color keys which reflect the rotational symmetry of the icosahedral quasicrystals in point group 235 and the point group 10 2 2 for the decagonal quasicrystals, as implemented in MTEX 5.2 [47].

3. Results and discussion

3.1. Microtexture of an icosahedrally quasicrystalline material

As described in the experimental section above, the quasicrystalline Ti40Zr40Ni20 sample was produced by suction casting of the alloy melt into a cold copper mould, resulting in a cylindrical casting. The rapid solidification involves locally changing temperature gradients and differing cooling rates, which influences the competitive growth of quasicrystal grains. Based on what is known about the general properties of casting processes, we can expect the largest qualitative differences between the edge of the cast sample and its center [48]. For an overview of other applications of EBSD in the field of solidification, see also [49]. In our casting setup, the edge region of the sample is dominated by the high heat transfer through the copper mould walls in Fig. 2(a), while the sample center is controlled by a different temperature gradient leading to the larger and more equiaxed grains in Fig. 2(b). In order to reveal the expected qualitative differences of the quasicrystal solidification near the sample edge compared to the center region, we investigated these two areas by EBSD using pattern matching to the experimental Kikuchi master reference.

The maps in Fig. 2 show the results of the orientation determination using the icosahedral Kikuchi master reference as determined in Fig. 1. The color key in Fig. 2(c) is applied to color the map points according to the crystallographic direction which aligns with a given direction in the sample system, leading to so-called “inverse pole figure maps” (“IPF-maps”). The measurement in Fig. 2(a) is near the sample edge, which is located at the left side of the map. The temperature gradient was directed from the cylinder side walls towards the inside of the cylindrical sample, i.e. to the right of the measured area

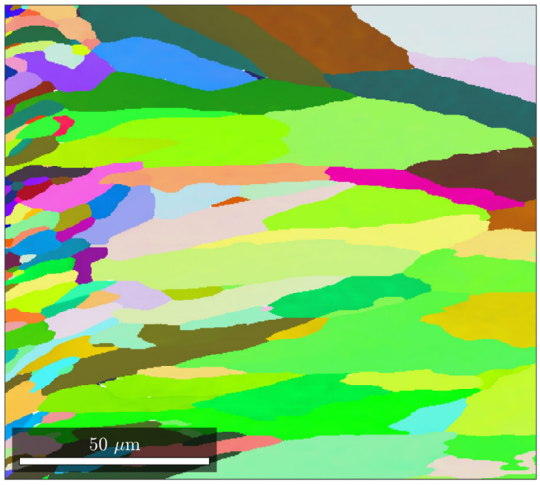

(a) sample edge region, direction of X-axis

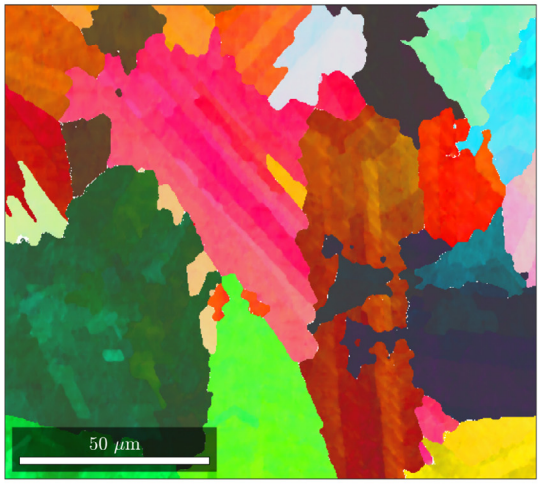

(b) sample center region, direction of Z-axis

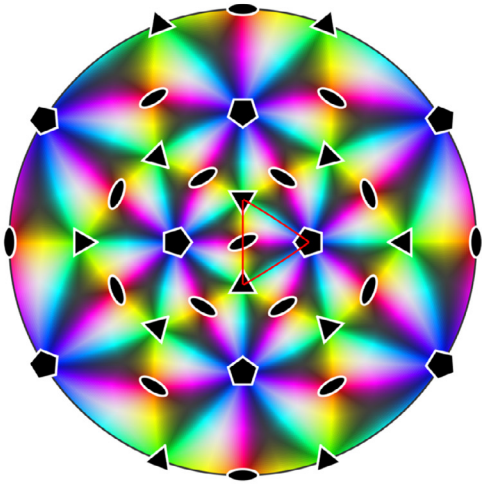

(c) color key for directions in point group 235

Fig. 2. Orientation analysis of two different sample regions at the edge (a) and near the center (b) of a Ti40Zr40Ni20 sample. The colors correspond to the relative alignment of the sample X-axis (a) and Z-axis (b), in the reference system of point group 235 (c). The fundamental sector used is outlined using red lines in (c). (For interpretation of the references to colour in this figure legend, the reader is referred to the web version of this article.)

along the sample's X-axis. This is why, in Fig. 2(a), we use an IPF-X map to correlate properties of the inter-grain microtexture with the temperature gradient during solidification. As is typical for a cast microstructure, the grains in the nucleation zone at the left edge of the map in Fig. 2(a) are of small size, and randomly oriented as seen by the random color variation. After a short distance of competitive growth, grains with a fast growing direction parallel to the temperature gradient become dominant. The mainly greenish color in Fig. 2 (a) indicates that a fast growing direction for this region is preferably parallel to one of the three-fold rotation axes, as can be seen in the color key in (c). The regions of grains with similar (in this case all green) colors suggest a systematic, fiber-like texture of these grains.

With a decreasing temperature gradient, the grains grow clearly larger, as can be seen in Fig. 2(b) for a sample region which is located in the center of the sample. The coloring used in Fig. 2(b) refers to the quasicrystal direction parallel to the sample Z-axis, which was chosen to reflect the local temperature gradient. The change of the gradient direction from along the X-axis in Fig. 2(a) to along the Z-axis in Fig. 2(b) is consistent with the fact that the investigated sample has been taken from the lower part of the cast, where the heat transfer direction in the sample center can be additionally affected by the bottom crucible plate. The red colors of the IPF-Z map shown in Fig. 2(b) now indicate a preferred growth along a two-fold rotation axis. Because the map in Fig. 2(b) does not allow a reliable prediction of a possible texture or preferred orientation due to the very low number of grains, in Fig. 3(a) we show a map which was collected from a larger area at a nearby position.

The grain boundaries which are visible in Fig. 3(a) suggest a dendritic growth which results in typical wavy or meandering boundaries. The pole figure in Fig. 3(b) displays the distribution of all directions parallel to two-fold rotation axes. The fiber axis in the center of the pole figure means that the majority of grains in the map rotate around one of the two-fold axes which is perpendicular to the surface of the investigated sample (i.e. parallel to the cylinder axis of the cast sample). We explicitly show by the filled circles the position of the two-fold axes for the mean orientation of all grains in Fig. 3(a). As can be estimated from the pole figure, the inter-grain misorientations cover a range of approximately $\pm 30^\circ$ around the mean.

In addition, we can also analyze the orientation variations *inside* the individual grains. For example, in Fig. 2(b) as well as Fig. 3(a) we observe a characteristic striation within the grains. These variations can be described quantitatively by the orientation deviation relative to the mean orientation in the grain. In Fig. 4, we show the intragranular misorientation analysis corresponding to the orientation maps in Fig. 2. The misorientations can be quantified by the value of the misorientation angles as seen in the left panels (a,d) of Fig. 4 and by the directions of the misorientation axes relative to the mean orientation of the grain shown in the middle panels (b,e). The corresponding color keys for the upper and lower hemispheres in Fig. 4(c,f) are used to describe the 3D directions of the misorientation axes and the misorientation angles in the sample coordinate system as described in [50] and as implemented in MTEX [47]. A preferential alignment of misorientation axes will be seen by clustering of the mapped directions which are shown by the black dots in Fig. 4(c,f).

In the misorientation maps from the edge of the sample in the upper part of Fig. 4, we find relatively continuous rotations within the grains, and no distinct subgrain boundaries are detectable, as is seen by the continuous color changes. However, the intragranular rotations indicate a clear correlation to the assumed fiber axis parallel to X because the misorientation axes cluster near the east-west axis in the hemispherical color key in Fig. 4(c).

We find a different situation in the central region of the sample, as shown in the lower panels (d,e,f) of Fig. 4. While the IPF-Z map in Fig. 2(b) and the pole figure in Fig. 3 indicated a fiber-like texture relative to the sample Z-axis, the color jumps seen in Fig. 4(e) suggest subgrain boundaries which do not show an obvious correlation to the

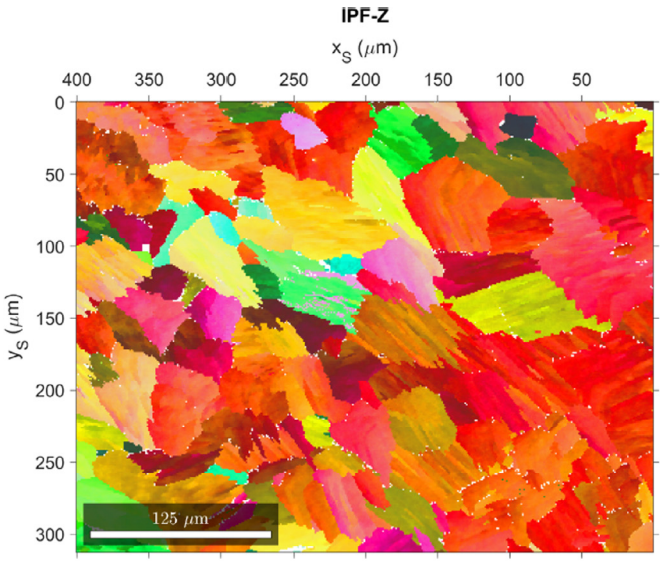

(a) IPF-Z map in central region of sample

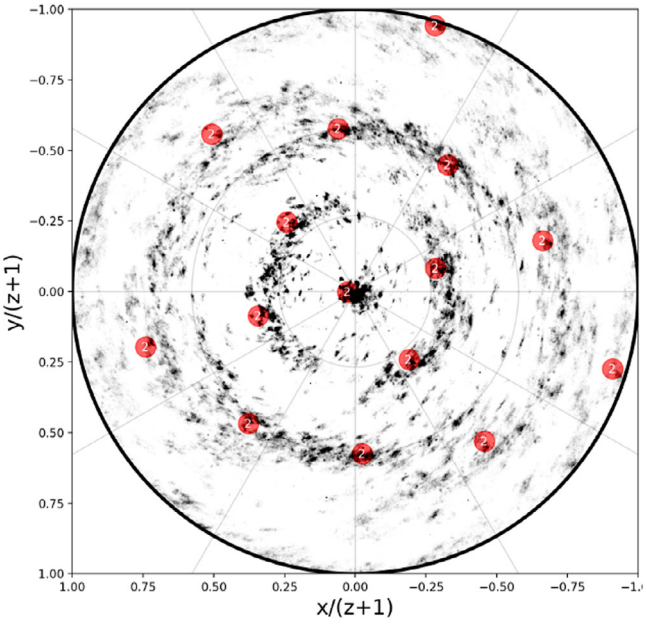

(b) pole figure of 2-fold axes

Fig. 3. EBSD pole figure analysis from the center region of the Ti40Zr40Ni20 sample. The markers for the two-fold symmetry axes in (b) are shown for the mean orientation of the measurements in (a). The orientation changes in the mapped area can be approximated by systematic rotations around the two-fold axis pointing nearly parallel to the sample Z-axis, as indicated by the red colors of the IPF-Z map in (a), see also the color key in Fig. 2(c). (For interpretation of the references to colour in this figure legend, the reader is referred to the web version of this article.)

observed fiber texture. Consequently, the misorientation axis distribution does not display any pole clustering in Fig. 4(f). The lath-like subgrains in Fig. 4(d) display nearly constant grey levels which reflects a systematic misorientation of these blocks. The colors in the misorientation axis map in Fig. 4(e) also suggest that the small blocks with a diameter of the thickness of the lathes are likely to correspond to lathes a well, which are directed out-of-plane, however. We expect

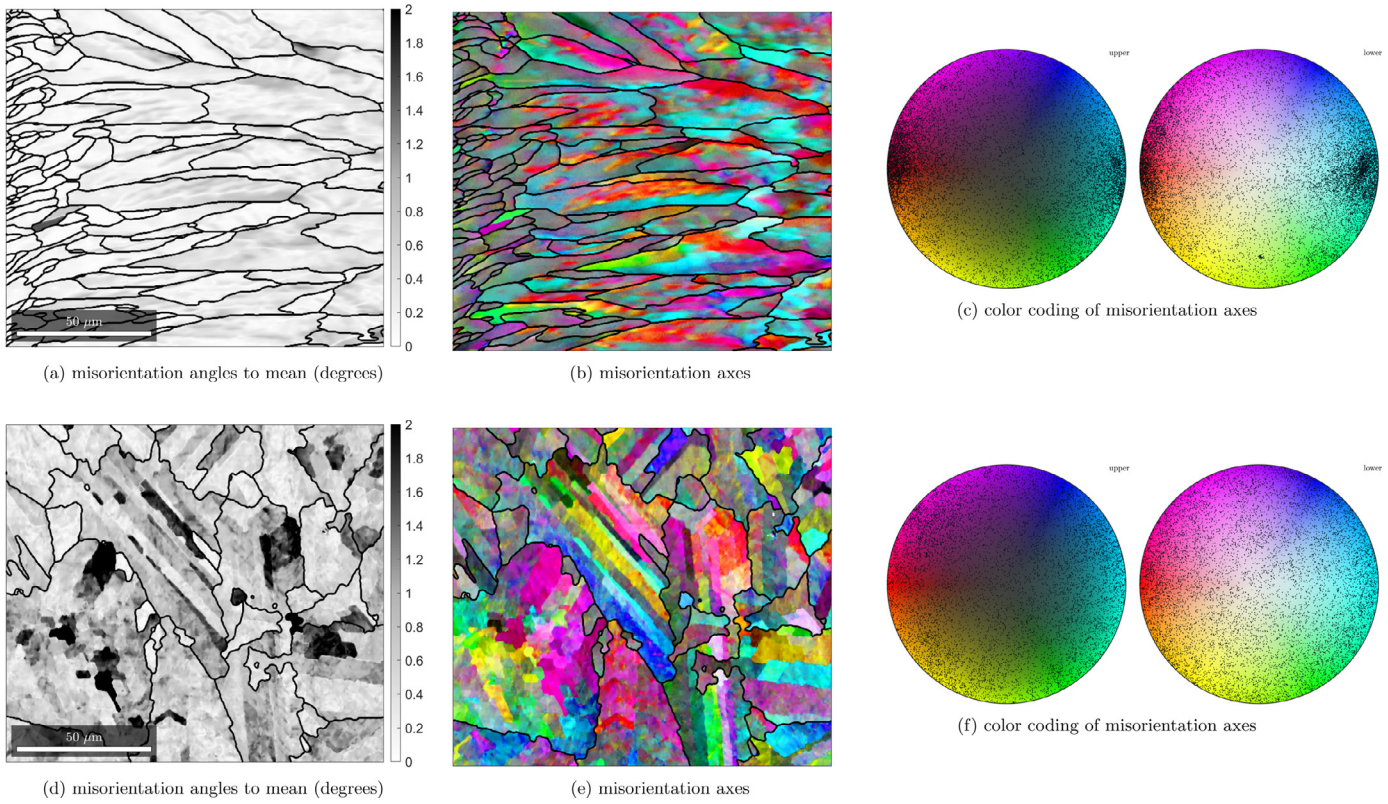

(a) misorientation angles to mean (degrees) (b) misorientation axes (c) color coding of misorientation axes

(d) misorientation angles to mean (degrees) (e) misorientation axes (f) color coding of misorientation axes

Fig. 4. Analysis of intragranular misorientations within the areas mapped in Fig. 2 (upper panels: edge region, lower panels: central region). The misorientations are quantified by their rotation angle (left panels a,d) and the directions of the misorientation axes (middle, b,e) with the corresponding hemispherical color keys and axis distributions in the sample coordinate system (right, c,f). The left/right color keys correspond to the rotation axes pointing towards the upper/lower hemisphere, for positive rotation angles. The grain boundaries with a minimum misorientation angle of 5° are shown as the black lines.

that more insight into the peculiar intragranular subtexture can be obtained by higher resolved EBSD measurements which could shed light on the possible role of minority phases and the formation of strain in the grains [51]. Specifically along the subgrain boundaries, Laves C14 and/or β-TiZr phases can occur, as these additional phases have been found previously by X-ray diffraction [23]. The local study of the distribution of the minority phases by EBSD in the future could also provide more general information on the rapid solidification process of the quasicrystalline phase with a related creation of local strains, because a rejection of chemical species is known to influence the attachment kinetics during quasicrystal growth [51,52].

3.2. Decagonal quasicrystals with a secondary phase

The results for the $Ti_{40}Zr_{40}Ni_{20}$ sample as discussed above showed that we can obtain detailed orientation information from quasicrystalline samples by using an experimentally generated Kikuchi pattern master reference. In the case of icosahedral quasicrystals, the generation of the Kikuchi master reference has relatively modest requirements, because the directions of all the symmetry axes in an icosahedral structure are fixed and do not depend on further parameters [25]. This is why we can generate the pattern master reference from a fundamental sector which is contained in a single experimental pattern under typical observation conditions, i.e. when the experimental pattern covers angular ranges in the order of 60 to 90°. In the following, we discuss the generation of a lower symmetry Kikuchi master reference for decagonal AlCoNi, and we demonstrate a combined phase discrimination and orientation determination for a sample of AlCoNi which contains an additional crystalline phase, Al_3Ni.

Due to the symmetry of the decagonal quasicrystals, it was necessary to use several experimental EBSD patterns to assemble the Kikuchi master reference. In a first step, a gnomonic montage as shown in Fig. 5(a) was generated from three overlapping patterns according to the 4-point correspondence approach described above. This combined gnomonic data covers an angular range of more than 90°, including the two-fold axes and the 10-fold axis. The angular distance between adjacent 2-fold axes in Fig. 5(a) is 18°. In the same way as for the previous example of the 5-fold quasicrystal, one only needs to identify 4 related points in two related gnomonic patterns in order to fix the relative projection between them. For the remapping of the experimental AlCoNi patterns to the Kikuchi sphere, we used the visible 10-fold axis and the 2-fold axes perpendicular to it, and we additionally identified the lattice plane traces of the (0 0 -1 -1 1) planes [53]. These lattice planes are inclined relative to the 10-fold axis and the inclination angle is dependent on the actual quasicrystal structure [54]. According to [53], the normals of these planes make an angle of 60.4° with the ten-fold axis of the AlCoNi quasicrystal, which fixes the angle with the zone axis which is marked with an 'X' in Fig. 5 at 29.6°. While we have taken the relevant angle from the literature, it would also be possible to determine the inclined plane angle from an EBSD-based goniometric measurement on a calibrated detection screen according to the rules of the gnomonic projection [26]. After application of the symmetry elements of the decagonal point group, the complete hemispherical Kikuchi data can be generated, as shown in Fig. 5(b). This decagonal experimental Kikuchi master reference was used for the orientation analysis described below. A fundamental sector of the *rotational* group 10 2 2 is shown by red lines in the stereogram of Fig. 5(c).

Concerning the reference system of the orientations determined using the experimental Kikuchi master reference, we note that two perpendicular two-fold reference axes in the equatorial plane of the crystal coordinate system are not symmetry-equivalent. This can be seen by comparison of the stereographic projection and the rotational color key in Fig. 5(b) and (c), respectively. Two non-equivalent

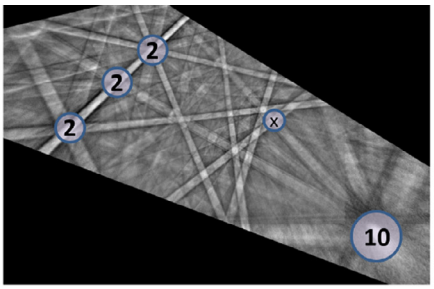

(a) reference axes in experimental data of AlCoNi

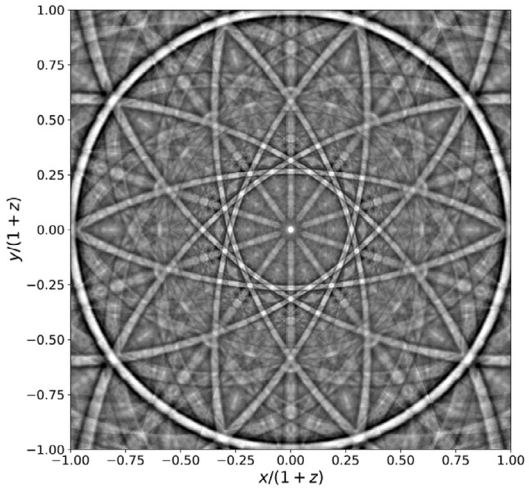

(b) stereographic projection for decagonal AlCoNi

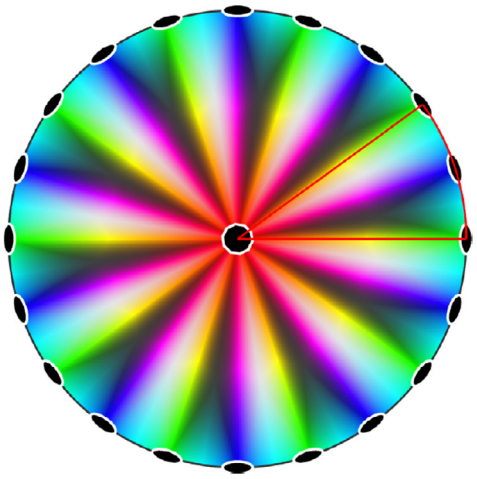

(c) color key for directions in decagonal quasicrystals

Fig. 5. Generation of the decagonal Kikuchi master reference for the analysis of the decagonal AlNiCo quasicrystal samples. (a) montage of gnomonic reference data with calibration directions, (b) stereographic projection and symmetrization of (a), (c) color key for rotational group 10 2 2, a fundamental sector is outlined by red lines.

definitions of orientation descriptions can result depending on the actual choice of the two-fold axes for the Cartesian reference system. These orientations differ by the value $\Delta\phi_1 = 18^\circ$ in the first Z-rotation Euler angle ϕ_1, i.e. the separation between two two-fold rotation axes. Concerning pattern matching in EBSD in general, this illustrates the necessity to clearly specify the chosen reference setting for the master data, i.e. similar to the orientation reference for conventional EBSD from hexagonal crystals, which can differ by $\Delta\phi_1 = 30^\circ$ in their reference orientation.

In Fig. 6, we present the results of a combined phase discrimination and orientation determination from the AlCoNi sample. We selected an area consisting of three large AlCoNi grains and a secondary phase, Al_3Ni, which is known to occur in the context of growth experiments of AlNiCo quasicrystals [55,56].

A representative EBSD pattern from AlCoNi is shown in Fig. 6(a). The Al_3Ni crystallized between the quasicrystal grain boundaries, which is seen in the map of the integrated BSE signal on the EBSD phosphor screen in Fig. 6(b). The regions of Al_3Ni show an approximately 2% smaller backscattering signal than the quasicrystalline AlCoNi regions.

The phase map of Fig. 6(c) was determined in two stages. In a first step, the orientations of the orthorhombic Al_3Ni phase were determined by a conventional Hough-based indexing using the EBSD system software (Esprit 1.94, Bruker Nano), which, however, left the quasicrystalline regions unindexed. This tentative phase assignment was then refined by pattern matching of the complete map against both (a) a dynamically simulated Kikuchi master reference for Al_3Ni and (b) the experimental AlCoNi Kikuchi master reference [39]. The phase at each map point was then assigned according to the fit with the highest normalized cross correlation coefficient which resulted in the phase map of Fig. 6(c). The pattern matching allowed a clear separation between Al3Ni and AlNiCo regions, with normalized cross correlation coefficients $r > 0.4$ for the best-fit phase and $r < 0.2$ for fits of the respective other phase at the same map point.

The local orientation changes in the sampled area are shown by the kernel average misorientation (KAM) map in Fig. 6(d), which indicates that the AlCoNi grains do not show any considerable subgrain structure. The precision of the orientation assignment, determined by both the inherent crystal quality and by the limits of pattern matching approach, can be estimated by the histogram of the KAM angles which is shown in the inset of Fig. 6(d). The KAM distribution has a unimodal shape with a maximum at $\approx 0.04^\circ$ and a median value of $\approx 0.05^\circ$, with 95% of all misorientation values included in a range $< 0.1^\circ$. These values indicate a very good quality of the quasicrystal, and also a high precision of the pattern matching procedure. The characteristic values of the KAM histogram which we determined are near the orientation resolution limits imposed by the available Kikuchi pattern resolution of 160 × 115 pixels [39]. Our results concerning the excellent quasicrystalline quality in the AlCoNi grains of the present sample are in agreement with observations based on X-ray diffraction measurements performed on perfect single quasicrystals [53].

In addition to the increased KAM values directly at the grain boundaries, the KAM map of Fig. 6(d) also indicates a substructure of regular low-angle rotations for the Al3Ni grain near the lower middle part of the map, which can also be seen in the BSE map of Fig. 6(b). For a comparison to the local orientation changes visible in the KAM maps, we show in Fig. 6(e), the grains in both phases using an IPF-X map coloring. In the region of Al_3Ni this indicates the presence of 6 grains with large angle boundaries. Taking into account the very limited number of measured grains, we cannot conclude, however, on

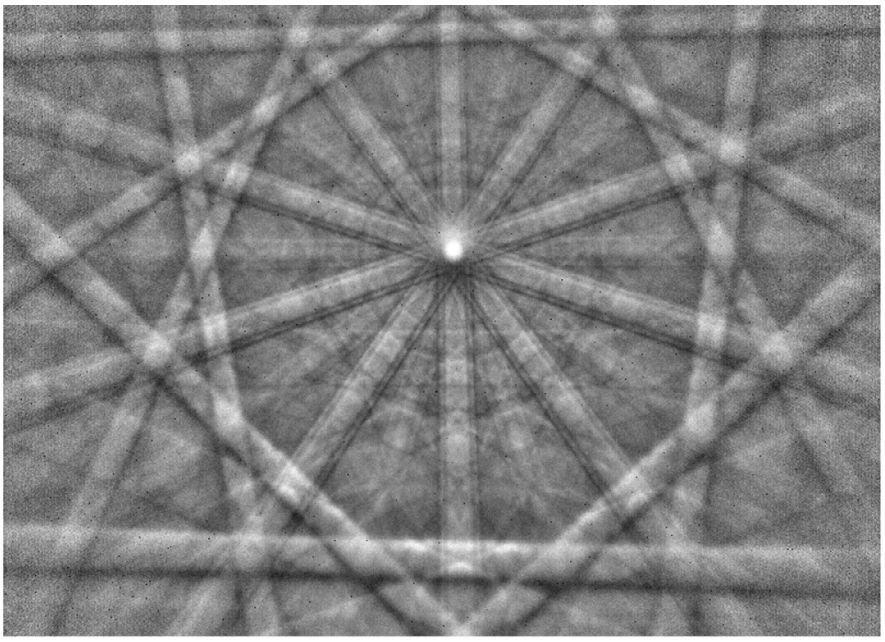

(a)

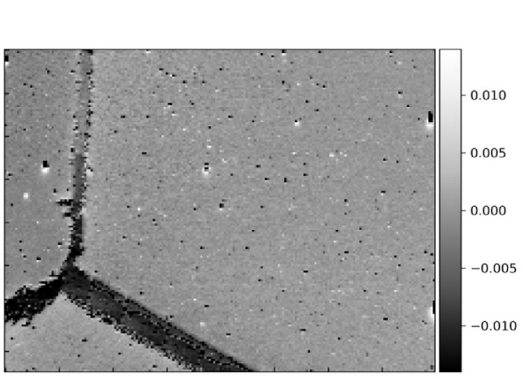

(b)

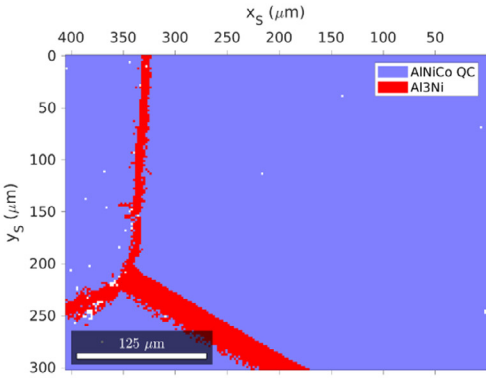

(c)

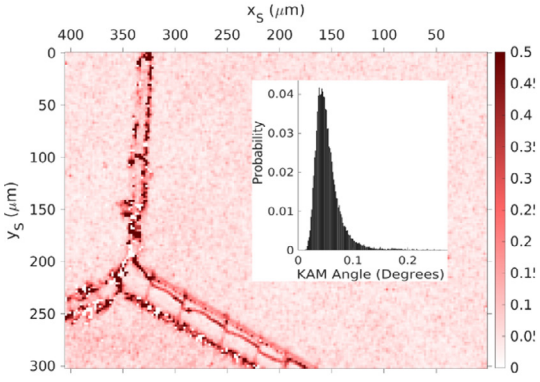

(d)

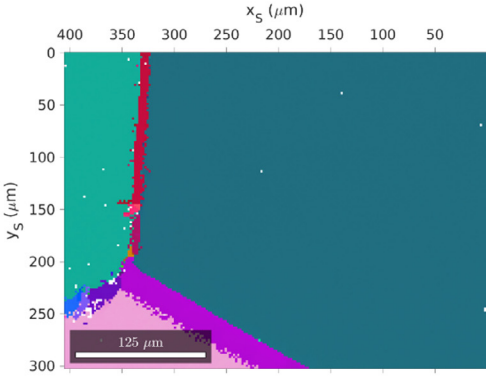

(e)

Fig. 6. Orientation mapping for the AlCoNi sample: (a) experimental Kikuchi pattern showing the 10-fold rotation axis of AlCoNi, (b) variation of the total BSE signal on the EBSD screen relative to the mean signal, (c) phase map, (d) Kernel Average Misorientation angles in degrees, the inset shows the histogram of the KAM angles, (e) orientation map with inverse pole figure (IPF-X) coloring.

any detailed orientation relationship between the AlCoNi grains and the Al_3Ni phase. The exact interpretation of the observed orientation features is beyond the topic of the present study, but the results of Fig. 6 illustrate the possibility to study of microstructures which are combined of conventional and quasicrystalline phases.

While the observed microstructure for the AlCoNi sample is much simpler than for the cast $Ti_{40}Zr_{40}Ni_{20}$ sample, this example demonstrates the combined use of several available approaches for EBSD phase discrimination and orientation determination: (a) the conventional, Hough-transform based approach of the commercial EBSD system, (b) the use of Kikuchi pattern simulations according to the dynamical theory of electron diffraction, as well as (c) pattern matching to an experimental Kikuchi master reference. The combination of these approaches will be especially useful for the investigation of possible orientation relationships between crystalline and quasicrystalline phases.

4. Summary and conclusion

We have presented an EBSD technique which enables phase discrimination and texture determination based on experimental reference patterns, without the use of pattern simulations. The necessary Kikuchi pattern master reference can be generated by application of known symmetries to experimental Kikuchi patterns covering a fundamental sector of the full Kikuchi sphere. Orientation analysis is then possible relative to the Kikuchi diffraction master data in a reference setting, which is preferably chosen in alignment with directions of symmetry axes. For the icosahedral quasicrystal analyzed here, these reference axes are chosen along the two-fold axes. Crystal orientations can be determined by template matching without explicit knowledge of the crystallographic indexing of lattice planes and directions. A subsequent orientation refinement delivers a comparable orientation precision as pattern matching to simulated data [39]. Experimental Kikuchi master references can take into account the distinguishing phenomenological effects of the observed phases, which include for example, the formation of HOLZ rings [8]. A proper inclusion of these effects in the Kikuchi master reference will contribute to a higher orientation precision and a more sensitive phase discrimination in the pattern matching process.

The EBSD approach based on experimental master references is best seen as an additional option which can be combined with other available methods for phase discrimination and orientation determination from Kikuchi patterns. In this way, EBSD analyses from complex materials can benefit from the combination of approaches which are tailored to extract the optimum amount of information from the available experimental data. For example, initial orientations of very similar phases in many cases can be obtained using a conventional, fast, approach based on the Hough transform [4], while a detailed phase assignment could be based on additional verification by dynamical pattern simulations [5] or by comparison to available experimental Kikuchi master references as presented here.

The limits of the EBSD approach presented here are set by effects which cannot be described in a simple reprojection of Kikuchi pattern templates from a single common master reference. For example, the so-called excess-deficiency effects [57] are related to the specific geometry of the incident beam and they can influence the assignment of polarity in non-centrosymmetric phases or lead to a systematic bias in the orientation determination. If patterns of a very similar orientation are compared, however, the experimental reference could also include the excess-deficiency effects and in this way lead to a higher reliability of polarity assignment in nanocrystalline structures, see e.g. [58]. The available precision of an experimental Kikuchi master reference will be also limited by the generation of the master reference itself. This depends, for example, on the precision of the relative alignment between several patterns which can be necessary to assemble the fundamental sector of the Kikuchi sphere for low symmetry phases. Also, pattern distortions other than those which are due to the gnomonic projection, need to be taken into account for a precise reprojection of experimental intensities to the spherical coordinate system of the Kikuchi master reference.

In addition to the quasicrystalline samples which were investigated in the present study, we expect that the discussed approach will be especially useful for texture analysis and phase discrimination in demanding materials like complex intermetallics, superlattice structures, as well as metastable materials, all of which can consist of ordered, partially disordered or deformed phases. Further possible applications include geological and biological materials, for which it can be difficult to obtain simulated patterns with a sufficiently detailed consideration of all experimental effects.

Declaration of Competing Interest

The authors declare that they have no known competing financial interests or personal relationships that could have appeared to influence the work reported in this paper.

Acknowledgments

We would like to thank P. Gille (Ludwig-Maximilians-University, Munich) for providing the AlCoNi quasi-crystal sample and M. Buchheim and R. Saliwan-Neumann (BAM Berlin) for sample preparation and data collection. This work was supported by the Polish National Agency for Academic Exchange (NAWA), grants PPI/APM/2018/1/00049/U/001 and PPN/ULM/2019/1/00068/U/00001 and by the German Research Foundation (DFG-388933555).

References

[1] A.J. Schwartz, M. Kumar, B.L. Adams, D.P. Field, Electron Backscatter Diffraction in Materials Science, Springer US, 2009, doi: 10.1007/978-0-387-88136-2.
[2] J.A. Venables, C.J. Harland, Electron back-scattering patterns - a new technique for obtaining crystallographic information in the scanning electron microscope, Phil. Mag. 27 (1973) 1193–1200, doi: 10.1080/14786437308225827.
[3] A. Winkelmann, G. Nolze, M. Vos, F. Salvat-Pujol, W.S.M. Werner, Physics-based simulation models for EBSD: advances and challenges, Proceedings of the IOP Conference Series: Materials Science and Engineering 109 (1) (2016) 012018, doi: 10.1088/1757-899X/109/1/012018.
[4] S.I. Wright, Fundamentals of Automated EBSD, in: Electron Backscatter Diffraction in Materials Science, Springer US, 2000, pp. 51–64, doi: 10.1007/978-1-4757-3205-4_5.
[5] A. Winkelmann, C. Trager-Cowan, F. Sweeney, A.P. Day, P. Parbrook, Many-Beam Dynamical Simulation of Electron Backscatter Diffraction Patterns, Ultramicroscopy 107 (2007) 414–421, doi: 10.1016/j.ultramic.2006.10.006.
[6] C. Maurice, K. Dzieciol, R. Fortunier, A method for accurate localisation of EBSD pattern centres, Ultramicroscopy 111 (2) (2011) 140–148, doi: 10.1016/j.ultramic.2010.10.007.
[7] P.G. Callahan, M. De Graef, Dynamical electron backscatter diffraction patterns. Part I: Pattern simulations, Microsc. Microanal. 19 (2013) 1255–1265, doi: 10.1017/S1431927613001840.
[8] J.R. Michael, J.A. Eades, Use of reciprocal lattice layer spacing in electron backscatter diffraction pattern analysis, Ultramicroscopy 81 (2) (2000) 67–81, doi: 10.1016/S0304-3991(99)00119-9.
[9] J.I. Goldstein, D.E. Newbury, P. Echlin, D.C. Joy, C.E. Lyman, E. Lifshin, L. Sawyer, J.R. Michael, Scanning Electron Microscopy and X-ray Microanalysis, Springer, Boston, 2003, doi: 10.1007/978-1-4615-0215-9.
[10] D.C. Joy, D.E. Newbury, D.L. Davidson, Electron channeling patterns in the scanning electron microscope, J. Appl. Phys. 53 (8) (1982) R81–R122, doi: 10.1063/1.331668.
[11] D.J. Dingley, K.Z. Baba-Kishi, V. Randle, Atlas of backscattering Kikuchi diffraction patterns, Inst. of Physics Publ. (1995).
[12] J. Guo, T. Sato, T. Hirano, A. Tsai, Solid liquid interface in the growth of a decagonal Al-72 Co-16 Ni-12 quasicrystal, J. Cryst. Growth 197 (4) (1999) 963–966, doi: 10.1016/S0022-0248(98)01165-8.
[13] A.-P. Tsai, Discovery of stable icosahedral quasicrystals: progress in understanding structure and properties, Chem. Soc. Rev. 42 (2013) 5352–5365, doi: 10.1039/C3CS35388E.
[14] A.-P. Tsai, C. Cui, Crystal Growth of Quasicrystals, in: T. Nishinaga (Ed.), Handbook of Crystal Growth, Ch. 26 (Second Edition), Elsevier, Boston, 2015, pp. 1113–1156, doi: 10.1016/B978-0-444-56369-9.00026-5.
[15] W. Steurer, Quasicrystals: what do we know? what do we want to know? what can we know? Acta Crystallograph. Sect. A 74 (1) (2018) 1–11, doi: 10.1107/S2053273317016540.
[16] D. Naumovi, P. Aebi, L. Schlapbach, C. Beeli, K. Kunze, T.A. Lograsso, D.W. Delaney, Formation of a stable decagonal quasicrystalline Al-Pd-Mn surface layer, Phys. Rev. Lett. 87 (2001) 195506, doi: 10.1103/PhysRevLett.87.195506.

[17] R. Tanaka, S. Ohhashi, N. Fujita, M. Demura, A. Yamamoto, A. Kato, A. Tsai, Application of electron backscatter diffraction (EBSD) to quasicrystal-containing microstructures in the Mg-Cd-Yb system, Acta Mater 119 (2016) 193–202, doi: 10.1016/j.actamat.2016.08.011.
[18] L. Bindi, C. Lin, C. Ma, P.J. Steinhardt, Collisions in outer space produced an icosahedral phase in the Khatyrka meteorite never observed previously in the laboratory, Sci. Rep. 6 (38117) (2016). doi:10.1038/srep38117.
[19] G. Kurtuldu, P. Jarry, M. Rappaz, Influence of Cr on the nucleation of primary Al and formation of twinned dendrites in Al Zn Cr alloys: can icosahedral solid clusters play a role? Acta Mater 61 (19) (2013) 7098–7108, doi: 10.1016/j.actamat.2013.07.056.
[20] F. Labib, S. Ohhashi, A.P. Tsai, Formation and crystallographic orientation study of quasicrystal, 2/1 and 1/1 approximants in Cd-Mg-Y system using electron backscatter diffraction (EBSD), Philos. Mag. 99 (2019) 1528–1550, doi: 10.1080/14786435.2019.1585589.
[21] S. Singh, W.C. Lenthe, M. De Graef, Many-beam dynamical scattering simulations for scanning and transmission electron microscopy modalities for 2D and 3D quasicrystals, Philos. Mag. (2019) 1–19, doi: 10.1080/14786435.2019.1605217.
[22] T. Kozieł, Estimation of cooling rates in suction casting and copper-mould casting processes, Arch. Metall. Mater. 60 (2) (2015) 767–771, doi: 10.1515/amm-2015-0204.
[23] J. Qiang, Y. Wang, D. Wang, M. Kramer, C. Dong, Ti–Zr–Ni bulk quasicrystals prepared by casting, Phil. Mag. Lett. 83 (7) (2003) 467–472, doi: 10.1080/0950083031000110298.
[24] B. Bauer, G. Meisterernst, J. Härtwig, T. Schenk, P. Gille, Czochralski growth and X-ray topographic characterization of decagonal AlCoNi quasicrystals, Phil. Mag. 86 (3–5) (2006) 317–322, doi: 10.1080/14786430500253927.
[25] D.B. Litvin, The icosahedral point groups, Acta Crystallograph. Sect. A 47 (2) (1991) 70–73, doi: 10.1107/S0108767390010054.
[26] G. Nolze, A. Winkelmann, Crystallometric and projective properties of Kikuchi diffraction patterns, J. Appl. Crystallogr. 50 (1) (2017) 102–119, doi: 10.1107/s1600576716017477.
[27] A. Winkelmann, G. Nolze, G. Cios, T. Tokarski, Mapping of local lattice parameter ratios by projective Kikuchi pattern matching, Phys. Rev. Mater. 2 (2018) 123803, doi: 10.1103/PhysRevMaterials.2.123803.
[28] T. Britton, J. Jiang, Y. Guo, A. Vilalta-Clemente, D. Wallis, L. Hansen, A. Winkelmann, A. Wilkinson, Tutorial: crystal orientations and EBSD - Or which way is up? Mater Charact. 117 (2016) 113–126, doi: 10.1016/j.matchar.2016.04.008.
[29] R. Hartley, A. Zisserman, Multiple View Geometry in Computer Vision, Cambridge University Press, 2003, doi: 10.1017/cbo9780511811685.
[30] J.A. Venables, R. Bin-Jaya, Accurate microcrystallography using electron back-scattering patterns, Philos. Mag. 35 (5) (1977) 1317–1332, doi: 10.1080/14786437708232955.
[31] S. Biggin, D.J. Dingley, A general method for locating the X-ray source point in Kossel diffraction, J. Appl. Crystallogr. 10 (5) (1977) 376–385, doi: 10.1107/s0021889877013806.
[32] B. Zitová, J. Flusser, Image registration methods: a survey, Image Vis Comput 21 (11) (2003) 977–1000, doi: 10.1016/s0262-8856(03)00137-9.
[33] R. Szeliski, Computer Vision, Springer, London, 2011, doi: 10.1007/978-1-84882-935-0.
[34] A.P. Day, Spherical EBSD, J. Microsc 230 (3) (2008) 472–486, doi: 10.1111/j.1365-2818.2008.02011.x.
[35] A.P. Day, Electron Backscatter Diffraction in Materials Science, 2nd ed., Springer Science + Business Media, New York, 2009. Ch. Spherical Kikuchi Maps and Other Rarities, pp. 65–80. doi:10.1007/978-0-387-88136-2_5
[36] T. Lühr, A. Winkelmann, G. Nolze, D. Krull, C. Westphal, Direct atom imaging by chemical-sensitive holography, Nano Lett. 16 (5) (2016) 3195–3201, doi: 10.1021/acs.nanolett.6b00524.
[37] C. Zhu, K. Kaufmann, K. Vecchio, Automated reconstruction of spherical Kikuchi maps, Microsc. Microanal. 25 (4) (2019) 912–923, doi: 10.1017/S1431927619000710.
[38] Y.H. Chen, S.U. Park, D. Wei, G. Newstadt, M.A. Jackson, J.P. Simmons, M. De Graef, A.O. Hero, A dictionary approach to electron backscatter diffraction indexing, Microsc. Microanal. 21 (03) (2015) 739–752, doi: 10.1017/s1431927615000756.
[39] G. Nolze, M. Jürgens, J. Olbricht, A. Winkelmann, Improving the precision of orientation measurements from technical materials via EBSD pattern matching, Acta Mater 159 (2018) 408–415, doi: 10.1016/j.actamat.2018.08.028.
[40] A. Yamamoto, Crystallography of quasiperiodic crystals, Acta Crystallograph. A 52 (4) (1996) 509–560, doi: 10.1107/s0108767396000967.
[41] A. Winkelmann, G. Nolze, Point-group sensitive orientation mapping of non-centrosymmetric crystals, Appl. Phys. Lett. 106 (7) (2015) 072101, doi: 10.1063/1.4907938.
[42] A. Winkelmann, G. Nolze, M. Himmerlich, A. Reichmann, Point group sensitive orientation mapping using EBSD, Proceedings of the 6th International Conference on Recrystallization and Grain Growth, Pittsburgh, USA, TMS, 2016. doi:10.13140/RG.2.1.1466.2648
[43] A. Winkelmann, T.B. Britton, G. Nolze, Constraints on the effective electron energy spectrum in backscatter Kikuchi diffraction, Phys. Rev. B 99 (2019) 064115, doi: 10.1103/PhysRevB.99.064115.
[44] W. Kossel, H. Voges, Röntgeninterferenzen an der Einkristallantikathode, Ann. Phys. 415 (8) (1935) 677–704, doi: 10.1002/andp.19354150802.
[45] D.J. Dingley, Theory and application of Kossel x-ray diffraction in the scanning electron microscope, Scanning 1 (2) (1978) 79–99, doi: 10.1002/sca.4950010201.
[46] X. Tao, A. Eades, Measurement and mapping of small changes of crystal orientation by electron backscattering diffraction, Microsc. Microanal. 11 (4) (2005) 341–353, doi: 10.1017/S1431927605050270.
[47] F. Bachmann, R. Hielscher, H. Schaeben, Texture Analysis with MTEX - a Free and Open Source Software Toolbox, Solid State Phenom. 160 (2010) 63–68, doi: 10.4028/www.scientific.net/SSP.160.63.
[48] M.E. Glicksman, Principles of Solidification, Springer, New York, 2011, doi: 10.1007/978-1-4419-7344-3.
[49] E. Boehm-Courjault, F. Gonzales, A. Jacot, F. Kohler, A. Mariaus, C. Niederberger, M.A. Salgado-Ordorica, M. Rappaz, EBSD: A powerful microstructure analysis technique in the field of solidification, J. Microsc. 233 (1) (2009) 160–169, doi: 10.1111/j.1365-2818.2008.03107.x.
[50] K. Thomsen, K. Mehnert, P.W. Trimby, A. Gholinia, Quaternion-based disorientation coloring of orientation maps, Ultramicroscopy 182 (2017) 62–67, doi: 10.1016/j.ultramic.2017.06.021.
[51] J. Gastaldi, T. Schenk, G. Reinhart, N. Mangelinck-Noel, V. Cristiglio, B. Billia, B. Grushko, J. Härtwig, H. Klein, J. Baruchel, H. Nguyen-Thi, In situ and real-time probing of quasicrystal solidification dynamics by synchrotron imaging, Phys. Rev. E 74 (2006) 031605, doi: 10.1103/PhysRevE.74.031605.
[52] I. Han, X. Xiao, A.J. Shahani, Probing the growth and melting pathways of a decagonal quasicrystal in real-time, Sci. Rep. 7 (1) (2017) 17407, doi: 10.1038/s41598-017-17821-0.
[53] P. Gille, G. Meisterernst, N. Faber, Inclined net plane faceting observed at Czochralski growth of decagonal AlCoNi quasicrystals, J. Cryst. Growth. 275 (1) (2005) 224–231, doi: 10.1016/j.jcrysgro.2004.10.088.
[54] A. Cervellino, T. Haibach, W. Steurer, Structure solution of the basic decagonal Al–Co–Ni phase by the atomic surfaces modelling method, Acta Crystallogr. Sect. B 58 (1) (2002) 8–33, doi: 10.1107/S0108768101018936.
[55] B. Grushko, D. Holland-Moritz, High-Ni Al-Ni-Co decagonal phase, Scr. Mater. 35 (10) (1996) 1141–1146, doi: 10.1016/1359-6462(96)00281-3.
[56] W. Wolf, B.O. Sitta, L.M. Martini, A.M. Jorge, C. Bolfarini, C.S. Kiminami, W.J. Botta, Effect of Cr addition on the formation of the decagonal quasicrystalline phase of a rapidly solidified Al-Ni-Co alloy, J. Alloys Compd. 707 (2017) 41–45, doi: 10.1016/j.jallcom.2016.10.050.
[57] Y. Kainuma, The theory of Kikuchi patterns, Acta Cryst. 8 (1955) 247, doi: 10.1107/S0365110X55000832.
[58] G. Naresh-Kumar, J. Bruckbauer, A. Winkelmann, X. Yu, B. Hourahine, T. Wang, C. Trager-Cowan, R.W. Martin, P.r. Edwards, Determining GaN nanowire polarity and its influence on light emission in the scanning electron microscope, Nano Lett. 19 (6) (2019) 3863–3870, doi: 10.1021/acs.nanolett.9b01054.